Performance Comparison of OFDM and OFDM-IM for 6G Wireless Networks

Sumit Sugandhi
Dept. of Electrical and Electronics
Auckland University of Technology
Auckland, New Zealand
sumit.sugandhi@autuni.ac.nz

Xue Jun Li
Dept. of Electrical and Electronics
Auckland University of Technology
Auckland, New Zealand
xuejun.li@aut.ac.nz

Peter Han Joo Chong
Dept. of Electrical and Electronics
Auckland University of Technology
Auckland, New Zealand
peter.chong@aut.ac.nz

***Abstract*—This paper presents a comparative performance analysis of conventional coded orthogonal frequency-division multiplexing (OFDM) and multiple-input multiple-output (MIMO) OFDM with index modulation (OFDM-IM) as candidate waveforms for future sixth-generation (6G) wireless communication systems. A Rayleigh fading channel model is considered, employing convolutional channel coding, M-QAM modulation ($M \in \{4, 16, 32, 64\}$), and minimum mean-square error (MMSE) equalization under identical bandwidth and transmit power constraints. Unlike classical OFDM, OFDM-IM activates only a subset of subcarriers within each sub-block, enabling additional information transmission through subcarrier indices while reducing average interference and spectral leakage. Simulation results demonstrate that OFDM-IM consistently outperforms conventional OFDM by achieving notable signal-to-noise ratio (SNR) gains at practical bit error rate (BER) levels, along with significantly improved energy efficiency and reduced out-of-band (OOB) emissions across all considered modulation orders. These performance advantages highlight the strong potential of OFDM-IM as an energy-efficient and spectrally compact waveform for emerging 6G applications, including ultra-reliable low-latency communications, massive machine-type communications, and spectrum-constrained Internet-of-Things uplink scenarios.**

***Index Terms*—6G, OFDM, Index Modulation, BER, Energy Efficiency, Rayleigh fading, QAM.**

I. Introduction

The rapid evolution of wireless communication systems, driven by high data-rate, low-latency, and massive connectivity requirements, has motivated the development of advanced multicarrier modulation techniques for fifth-generation (5G) and beyond networks [1], [2]. Orthogonal Frequency Division Multiplexing (OFDM) is widely adopted in standards such as fourth-generation Long Term Evolution (4G LTE) and fifth-generation New Radio (5G NR) owing to its robustness against frequency-selective fading and efficient Fast Fourier Transform (FFT)-based implementation [3]. However, conventional OFDM struggles to satisfy emerging sixth-generation (6G) demands, particularly for massive Internet of Things (IoT) connectivity, asynchronous transmission, and reliable communication in high-mobility environments [1], [4].

Orthogonal Frequency Division Multiplexing with Index Modulation (OFDM-IM) has emerged as a promising alternative, which jointly encodes information in modulation symbols and active subcarrier indices to improve BER performance and robustness to inter-carrier interference [5]. Several variants have been proposed to further improve the performance. Affine Frequency Division Multiplexing with Index Modulation (AFDM-IM) enhances BER and energy efficiency (EE) in high-mobility scenarios through chirp-based signaling and adaptive power allocation [6], while Multi-Mode OFDM-IM (MM-OFDM-IM), along with its High-Dimensional (HM-OFDM-IM) and Rotated Fading-resistant (RF-HM-OFDM-IM) extensions, achieves improved minimum distance and full diversity over Rayleigh fading channels [7]. In parallel, reliability and spectral efficiency have been enhanced through channel-coded and adaptive OFDM frameworks. Channel-coded OFDM employs Forward Error Correction (FEC) schemes such as Low-Density Parity-Check (LDPC), Turbo, and Polar codes to improve robustness over Additive White Gaussian Noise (AWGN) and fading channels [8]. Adaptive Modulation OFDM exploits Channel State Information (CSI) to dynamically adjust modulation orders [9], while Multiple-Input Multiple-Output Orthogonal Frequency Division Multiplexing (MIMO-OFDM) leverages spatial diversity and multiplexing gains as a cornerstone of modern wireless standards [10].

Recent studies also show that index-based OFDM variants, including OFDM with Subcarrier Number Modulation (OFDM-SNM) and OFDM with Hybrid Number and Index Modulation (OFDM-HNIM), provide substantial BER and energy efficiency gains, especially for low-order modulations such as Binary Phase Shift Keying (BPSK) [11], [12]. To mitigate OFDM-IM performance degradation at higher modulation orders, Lower-Order Modulation-assisted OFDM-IM (LOFDM-IM), deep learning-assisted detection, and hybrid schemes combining OFDM-IM with Non-Orthogonal Multiple Access (NOMA) and cooperative relaying have been proposed, demonstrating improved BER, throughput, and reliability for 5G and beyond systems [13], [14], [15]–[18].

Despite extensive studies on OFDM and its variants, a fair performance comparison between conventional OFDM and OFDM-IM under identical bandwidth and transmit power constraints remains limited. This work is motivated by the need to clarify whether the additional index-domain signaling in OFDM-IM translates into tangible gains in reliability, energy efficiency, and spectral containment for future 6G-oriented wireless systems.

This paper presents a comprehensive comparison between conventional OFDM and OFDM-IM as candidate modulation techniques for future wireless communication systems. By evaluating their performance in terms of energy efficiency, power spectral density, BER, and signal-to-noise ratio (SNR) under Rayleigh fading conditions, the study highlights their suitability for emerging 6G applications, including massive IoT and ultra-reliable low-latency communications (URLLC). The remainder of this paper is organized as follows. Section II describes the system model of OFDM and OFDM-IM with explanations. Section III presents the mathematical models of both modulation techniques. Section IV discusses the simulation results and identifies future research directions. Finally, Section V concludes the paper and outlines potential directions for further investigation.

II. System Model

This section presents the signal model of a 2×2 MIMO communication system operating over a frequency-selective Rayleigh fading channel with AWGN. Both OFDM and OFDM-IM are evaluated under the same MIMO configuration with Nt = Nr = 2 transmit and receive antennas to ensure a fair comparison.

A. OFDM Signal Model

OFDM is a multicarrier transmission technique in which a high-rate data stream is divided into multiple lower-rate parallel streams, each transmitted over orthogonal subcarriers. The orthogonality ensures that the subcarriers overlap in frequency without causing inter-carrier interference (ICI), thereby achieving high spectral efficiency and robustness against frequency-selective fading. OFDM forms the basis of several advanced variants designed to further improve flexibility, spectral efficiency, energy efficiency, and reliability [19]. In a conventional OFDM system, a block of modulated symbols $\mathbf{x} = [x_0, x_1, \ldots, x_{N_c-1}]^T$ is transmitted over N_c orthogonal subcarriers. The time-domain signal is obtained via an N_c-point inverse fast Fourier transform (IFFT)

$$\mathbf{s} = \mathbf{F}^{-1}\mathbf{x}, \tag{1}$$

where $\mathbf{F}^{-1}$ denotes the IFFT matrix. A cyclic prefix (CP) of length L_{cp} is appended to mitigate inter-symbol interference (ISI).

After CP removal and fast Fourier transform (FFT) at the receiver, the frequency-domain received signal is given by

$$\mathbf{y} = \mathbf{H}\mathbf{x} + \mathbf{n}, \tag{2}$$

where $\mathbf{H} = \mathrm{diag}(h_0, h_1, \ldots, h_{N_c-1})$ represents the frequency-domain Rayleigh fading channel and $\mathbf{n}$ denotes AWGN.

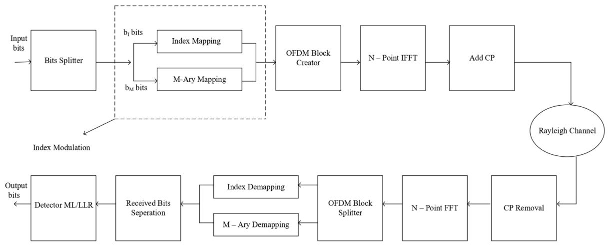

Fig. 1. Block Diagram of OFDM-IM

B. OFDM-IM Signal Model

Different from regular OFDM under which all the subcarriers carry data symbols, but in OFDM-IM, only some subcarriers are active at any given time. In particular, the indices (on which subcarriers are active) also carry data. This method not only boosts spectral and energy efficiency but can also reduce errors, since fewer subcarriers are transmitting at once, lowering interference and power consumption [20].

In OFDM-IM, as shown in Fig. 1, the N_c subcarriers are partitioned into $G = N_c/N$ groups, each consisting of N subcarriers. In each group, only K subcarriers are activated, whereas the remaining $N - K$ subcarriers remain inactive. For each subblock, the incoming bitstream is divided into

$$b_I = \left\lfloor \log_2 \binom{N}{K} \right\rfloor \tag{3}$$

index bits and

$$b_M = K \log_2(M) \tag{4}$$

modulation bits. The index bits select the active subcarrier set $\mathcal{I} = \{i_1, \ldots, i_K\}$, while the modulation bits are mapped to M-ary symbols.

The resulting OFDM-IM subblock $\mathbf{x}_g$ is expressed as

$$x_g(n) = \begin{cases} s_k, & n \in \mathcal{I} \\ 0, & \text{otherwise}, \end{cases} \tag{5}$$

where s_k denotes an M-ary symbol. All subblocks are concatenated to form the OFDM-IM frequency-domain block, followed by IFFT and CP insertion similar to conventional OFDM.

C. Receiver and Detection

After CP removal and FFT, the received OFDM-IM signal is modeled as

$$\mathbf{y} = \mathbf{H}\mathbf{x} + \mathbf{n}. \tag{6}$$

Frequency-domain equalization is performed using a minimum mean square error (MMSE) detector

$$\hat{\mathbf{x}} = \left(\mathbf{H}^H\mathbf{H} + \sigma_n^2\mathbf{I}\right)^{-1}\mathbf{H}^H\mathbf{y}, \tag{7}$$

where σ_n^2 denotes the noise variance.

TABLE I
SYSTEM SIMULATION PARAMETERS FOR OFDM AND OFDM-IM

S.N.	Parameter	Value
1	Number of Subcarriers (N_c)	64
2	Subcarrier Group Size (N)	4
3	Active Subcarriers per Group (K)	2
4	Groups per OFDM Block ($G = N_c/N$)	16
5	Modulation Order (M)	QPSK / 16-QAM / 32-QAM / 64-QAM
6	FFT Size	64
7	Channel Tap (L_h)	4
8	Cyclic Prefix Length (L_{cp})	16
9	Equalization Technique	MMSE

Index detection and symbol demodulation are jointly performed using maximum-likelihood (ML) or log-likelihood-based metrics. The detected indices and symbols are finally mapped back to reconstruct the transmitted bitstream.

III. SIMULATION SETUP

This section presents the complete mathematical formulation of a 2×2 MIMO OFDM-IM system with convolutional coding, M-QAM modulation, Rayleigh fading, and MMSE equalization. QAM modulation orders are $M = \{4, 16, 32, 64\}$. The OFDM-IM system uses a total of $N_c = 64$ subcarriers, divided into subblocks of size $N = 4$, with $K = 2$ active subcarriers per subblock. The key simulation parameters of the system for both OFDM and OFDM-IM are given in Table I. The total number of groups is given as $G = N_c/N$.

In each group, K subcarriers are activated. The system employs $N_t = N_r = 2$ transmit and receive antennas. Each channel has L_h taps, and a cyclic prefix (CP) of length $CP \geq L_h - 1$ is appended to each OFDM symbol.

To ensure a fair comparison between OFDM and OFDM-IM, both schemes are evaluated under identical bandwidth and average transmit power constraints. The average transmit power is normalized such that the total energy per OFDM symbol is equal for both schemes. Specifically, the per-symbol energy is set to $E_s = 1$, and since OFDM-IM activates only $K = 2$ out of $N = 4$ subcarriers per group, the active symbols are scaled to maintain the same total average power as conventional OFDM, where all $N_c = 64$ subcarriers are active. This normalization ensures that any observed performance differences are solely attributed to the structural advantages of index modulation rather than power allocation disparities.

A. Transmitter Model

Let the transmitted frequency-domain OFDM-IM block from transmit antenna t be

$$\mathbf{X}_t = \big[X_t(0), X_t(1), \ldots, X_t(N_c - 1)\big]^T \tag{8}$$

A rate-$\frac{1}{2}$ convolutional encoder maps the input bit sequence $\mathbf{b} = [b[0], b[1], \ldots]^T$ to the coded sequence $\mathbf{b}_c$ according to the trellis T of the encoder:

$$\mathbf{b}_c = \mathcal{E}(\mathbf{b}; T), \tag{9}$$

where $\mathcal{E}(\cdot)$ represents the convolutional encoding operation. The coded bits are partitioned per OFDM-IM group into index bits $\mathbf{b}_g^{(\mathrm{idx})}$ and modulation bits $\mathbf{b}_g^{(\mathrm{mod})}$. Each QAM symbol carries $m = \log_2 M$.

bits, and the normalized constellation is defined as

$$\mathcal{S} = \{s_1, s_2, \ldots, s_M\}, \quad \mathbb{E}[|s|^2] = E_s \tag{10}$$

For each group $g \in \{1, \ldots, G\}$, the set of subcarrier indices is

$$\mathcal{I}_g = \{(g-1)N, \ldots, gN - 1\} \tag{11}$$

K indices in $\mathcal{I}_g$ are activated. There are $\binom{N}{K}$ possible activation patterns. The index bits are mapped to an activation set $\mathcal{A}_g \subset \mathcal{I}_g$ as

$$\mathbf{b}_g^{(\mathrm{idx})} \longrightarrow \mathcal{A}_g \tag{12}$$

The transmitted symbol on subcarrier k from antenna t is

$$X_t(k) = \begin{cases} s \in \mathcal{S}, & k \in \mathcal{A}_g, \\ 0, & \text{otherwise.} \end{cases} \tag{13}$$

The total number of bits transmitted per OFDM symbol is

$$R_{\text{bits/sym}} = G\big(b_I + bm\big), \quad b_I = \lfloor \log_2 \binom{N}{K} \rfloor \tag{14}$$

The time-domain OFDM symbol is obtained via IFFT:

$$\mathbf{x}_t = \mathrm{IFFT}\{\mathbf{X}_t\}. \tag{15}$$

A cyclic prefix of length CP is appended as

$$\mathbf{x}_{\mathrm{cp},t} = \big[x_t(N_c - CP), \ldots, x_t(N_c - 1), \\ x_t(0), \ldots, x_t(N_c - 1)\big]^T \tag{16}$$

B. MIMO Rayleigh Fading Channel (Receiver Model)

The channel from transmit antenna t to receive antenna r has L_h taps:

$$h_{r,t}[l] \sim \mathcal{CN}\left(0, \frac{1}{L_h}\right), \quad l = 0, \ldots, L_h - 1. \tag{17}$$

The received time-domain signal at antenna r is

$$y_r[n] = \sum_{t=1}^{N_t} \sum_{l=0}^{L_h - 1} h_{r,t}[l]\, x_{\mathrm{cp},t}[n - l] + w_r[n], \tag{18}$$

where $w_r[n] \sim \mathcal{CN}(0, N_0)$ is AWGN.

After CP removal and FFT, the frequency-domain received signal is

$$Y_r(k) = \sum_{t=1}^{N_t} H_{r,t}(k) X_t(k) + W_r(k), \tag{19}$$

where the frequency-domain channel coefficients are

$$H_{r,t}(k) = \sum_{l=0}^{L_h-1} h_{r,t}[l]\, e^{-j2\pi kl/N_c} \tag{20}$$

For each subcarrier k, the MIMO channel matrix is

$$\mathbf{H}(k) = \begin{bmatrix} H_{1,1}(k) & H_{1,2}(k) \\ H_{2,1}(k) & H_{2,2}(k) \end{bmatrix}. \tag{21}$$

The MMSE equalization filter is

$$\mathbf{W}(k) = \big(\mathbf{H}^H(k)\mathbf{H}(k) + \frac{N_0}{E_s}\mathbf{I}\big)^{-1}\mathbf{H}^H(k), \tag{22}$$

and the equalized symbols are

$$\hat{\mathbf{X}}(k) = \mathbf{W}(k)\mathbf{Y}(k). \tag{23}$$

C. Soft Demodulation and Viterbi Decoding

For each QAM symbol, the Euclidean distance metric is

$$d(s) = \big|\hat{X}(k) - s\big|^2, \quad s \in \mathcal{S} \tag{24}$$

Using the max-log approximation, the log-likelihood ratio (LLR) of the i-th modulation bit is

$$\mathrm{LLR}(b_i) \approx \frac{1}{\sigma^2}\Big(\min_{s\in\mathcal{S}_0^i} d(s) - \min_{s\in\mathcal{S}_1^i} d(s)\Big), \tag{25}$$

where $\mathcal{S}_0^i$ and $\mathcal{S}_1^i$ are the sets of constellation points corresponding to bit values 0 and 1, respectively.

For index bits, the LLR is computed as

$$\Lambda(a) = \min_{s\in\mathcal{S}} \big|\hat{X}(k_a) - s\big|^2, \tag{26}$$

$$\mathrm{LLR}_{\mathrm{idx}}(b_i) \approx \frac{1}{\sigma^2}\Big(\min_{a\in\mathcal{A}_0^i} \Lambda(a) - \min_{a\in\mathcal{A}_1^i} \Lambda(a)\Big) \tag{27}$$

For soft Viterbi decoding, the LLRs are quantized:

$$q = \mathrm{clip}\Big(\big\lfloor -\mathrm{LLR}\cdot 2^{N_s-1}/L_{\max}\big\rfloor, q_{\min}, q_{\max}\Big), \tag{28}$$

where the negative sign ensures compatibility with the Viterbi decoder. Finally, the decoded bit sequence is

$$\hat{\mathbf{b}} = \arg\max_{\mathbf{b}} \Pr(\mathbf{b} \,|\, \mathbf{q}, T), \tag{29}$$

where $\mathbf{q}$ is the sequence of soft inputs and T is the convolutional encoder trellis.

D. Energy Efficiency

Assuming average energy per QAM symbol equals E_s, OFDM-IM uses

$$E_{\text{OFDM-IM}} = GKE_s, \tag{30}$$

while OFDM uses

$$E_{\text{OFDM}} = GNE_s. \tag{31}$$

Energy efficiency (bits per unit energy) becomes

$$\eta_{\text{OFDM-IM}} = \frac{B_{\text{OFDM-IM}}}{E_{\text{OFDM-IM}}} = \frac{b_i + Kb_s}{KE_s}, \tag{32}$$

$$\eta_{\text{OFDM}} = \frac{B_{\text{OFDM}}}{E_{\text{OFDM}}} = \frac{b_s}{E_s}. \tag{33}$$

With normalized symbol energy $E_s = 1$, these reduce to

$$\eta_{\text{OFDM-IM}} = \frac{b_i}{K} + b_s, \qquad \eta_{\text{OFDM}} = b_s. \tag{34}$$

Thus,

$$\eta_{\text{OFDM-IM}} - \eta_{\text{OFDM}} = \frac{b_i}{K}, \tag{35}$$

showing OFDM-IM is more energy-efficient whenever $b_i > 0$, i.e.,

$$\binom{N}{K} \geq 2. \tag{36}$$

E. Power Spectral Density (PSD) Formulation

To analyze the spectral characteristics of both OFDM and OFDM-IM, the discrete-time Fourier transforms (DTFTs) of the transmitted sequences are given by

$$X_{\text{OFDM}}(f) = \sum_n x_{\text{OFDM}}[n]e^{-j2\pi fn}, \tag{37}$$

$$X_{\text{OFDM-IM}}(f) = \sum_n x_{\text{OFDM-IM}}[n]e^{-j2\pi fn}. \tag{38}$$

The magnitude of the DTFT represents how the signal power is distributed across the frequency domain. To enable a fair comparison between both schemes, the PSDs are normalized by the maximum spectral amplitude, yielding

$$P_{\text{OFDM}}(f) = 20\log_{10}\left(\frac{|X_{\text{OFDM}}(f)|}{\max_f |X_{\text{OFDM}}(f)|}\right), \tag{39}$$

$$P_{\text{OFDM-IM}}(f) = 20\log_{10}\left(\frac{|X_{\text{OFDM-IM}}(f)|}{\max_f |X_{\text{OFDM-IM}}(f)|}\right). \tag{40}$$

With the parameters in Table I, since OFDM activates all $N_c = 64$ subcarriers uniformly, it produces a fully populated spectrum. In contrast, OFDM-IM activates only $K = 2$ of every $N = 4$ subcarrier per group, resulting in a spectrally sparse structure. This selective activation modifies the time-domain signal $x_{\mathrm{IM}}[n]$ and induces different spectral leakage characteristics compared to conventional OFDM.

The normalized PSD expressions above therefore highlight the differences in spectral shaping arising from subcarrier activation patterns rather than total transmit power, enabling a clear comparison of OFDM and OFDM-IM in terms of frequency-domain behavior.

IV. Results and Discussion

Fig. 2 shows the BER performance of conventional OFDM and the proposed OFDM-IM system was evaluated over a Rayleigh multipath channel for M-QAM modulation, using 64 subcarriers and 10,000 OFDM symbols per SNR point. For conventional OFDM, the BER decreases monotonically with increasing SNR, with 4-QAM achieving approximately 4.7×10^{-7} at 10 dB, while 16-QAM, 32-QAM, and 64-QAM require higher SNRs of around 12 dB, 14 dB, and 16 dB, respectively, to reach comparable performance. At SNR=30 dB, the BER further decreases to 2.02×10^{-4}, 7.1×10^{-4}, and 9.97×10^{-4} for 16-QAM, 32-QAM, and 64-QAM, reflecting the theoretical trends of QAM over

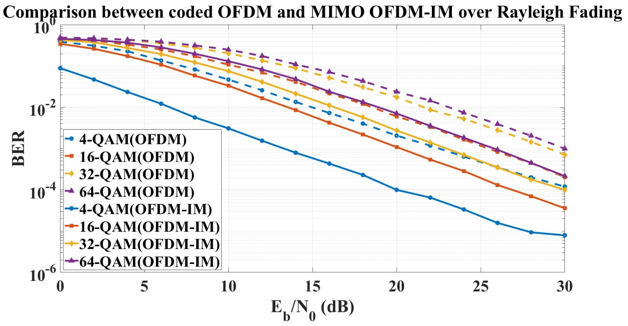

Fig. 2. BER comparison of conventional OFDM and OFDM-IM over Rayleigh channel for various QAM orders

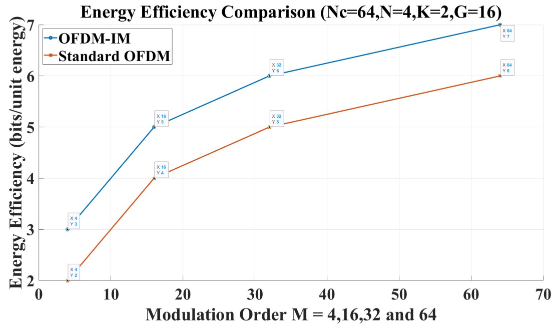

Fig. 3. Energy efficiency comparison of OFDM vs OFDM-IM

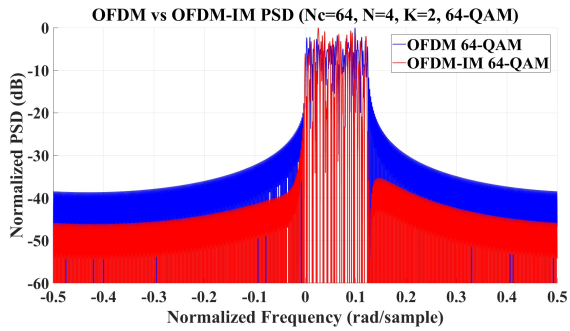

Fig. 4. Normalized PSD comparison of OFDM vs OFDM-IM

Rayleigh fading, with minor deviations due to the OFDM waveform structure.

In contrast, the OFDM-IM system, which activates only a subset of subcarriers per group (2 active subcarriers in groups of 4), conveys additional information via subcarrier indices. For 4-QAM, the BER drops rapidly from 8.87×10^{-2} at SNR=0 dB to the order of 10^{-6} at SNR=30 dB, highlighting high reliability due to the large Euclidean distance between constellation points. Higher-order modulations exhibit larger initial BERs because of denser constellations and index detection errors, with 16-QAM, 32-QAM, and 64-QAM starting at approximately 0.35, 0.43, and 0.46 at SNR=0 dB, respectively, and decreasing to 3.59×10^{-5}, 1.0×10^{-4}, and 2.16×10^{-4} at SNR=30 dB as shown in Fig. 2. These trends illustrate the inherent trade-off in OFDM-IM between spectral efficiency and reliability: lower-order modulations offer superior error performance, whereas higher-order schemes enable higher throughput but require higher SNR for comparable reliability. Overall, the results confirm that OFDM-IM effectively leverages both the subcarrier index and the symbol domains, providing robust error performance for moderate SNRs while supporting high spectral efficiency at elevated modulation orders.

Fig. 3 presents the energy efficiency comparison between conventional OFDM and OFDM-IM. OFDM-IM consistently outperforms conventional OFDM across all modulation orders. The achievable rate per subblock is $2\log_2 M$ bits for conventional OFDM and $(2\log_2 M + 2)$ bits for OFDM-IM. Since both schemes operate at identical average transmit energy, the energy efficiency advantage stems directly from the additional 2 index bits conveyed per subblock, corresponding to 32 extra bits per OFDM symbol at no additional power cost.

At $M = 4$, OFDM-IM achieves 3 bits/J compared to 2 bits/J for conventional OFDM, resulting in a 50% improvement. The relative gain gradually reduces with increasing M (25% at $M = 16$, 20% at $M = 32$, and approximately 16.7% at $M = 64$), following the theoretical efficiency ratio of $(1 + 1/\log_2 M)$. This behavior confirms that the energy efficiency benefits of OFDM-IM are most significant in low-to-moderate spectral efficiency regimes, which are prevalent in energy-constrained scenarios such as Internet of Things (IoT) devices, massive machine-type communications (mMTC), and uplink transmission in 5G and beyond-5G systems. Therefore, under practical constellation sizes, the $(4, 2)$ OFDM-IM scheme delivers substantial energy savings without requiring additional transmit power or bandwidth, reinforcing its strong potential for green and sustainable wireless communication systems.

Fig. 4 illustrates the normalized power spectral density (PSD) of conventional OFDM and OFDM-IM, both employing 64-QAM modulation with identical average transmit power. A key observation is that OFDM-IM exhibits significantly lower OOB emissions compared to conventional OFDM. In the transition bands ($|\tilde{f}| > 0.35$), the normalized PSD of OFDM-IM lies consistently below that of conventional OFDM by 5–15 dB, demonstrating a clear and measurable reduction in spectral leakage into adjacent frequency bands due to the partial subcarrier activation structure of OFDM-IM.

This desirable spectral containment property arises from the inherent structure of OFDM-IM. Since exactly $k = 2$ out of $n = 4$ subcarriers are deactivated in every subblock, the transmitted signal experiences a form of built-in partial subcarrier suppression. This randomness in activation patterns across subblocks disrupts the strong correlation between adjacent OFDM symbols that is present in conventional OFDM, thereby reducing large peak excursions in the time domain and suppressing high-frequency sidelobes in the frequency domain.

V. Conclusion

The necessity of this study lies in addressing a critical gap between theoretical promises of index modulation and practical waveform evaluation for future wireless systems. By providing a controlled system-level comparison under realistic channel conditions, this work clearly quantifies the tangible benefits of OFDM-IM over legacy OFDM. Simultaneous improvements in reliability, energy efficiency, and spectral containment directly align with the stringent requirements of emerging 6G use cases, including ultra-reliable low-latency communications, massive machine-type communications, and energy-constrained IoT uplinks. A comprehensive and fair comparative analysis of conventional OFDM and OFDM with index modulation (OFDM-IM) under identical bandwidth and average transmit power constraints over Rayleigh fading channels. Using a widely adopted ($n = 4, k = 2$) OFDM-IM configuration and practical modulation orders ranging from 4-QAM to 64-QAM, the study systematically evaluated BER, SNR gain, energy efficiency, and spectral characteristics. The results demonstrate that OFDM-IM consistently outperforms classical OFDM by delivering 2—4 dB SNR gain in BER, specifically indicating that OFDM-IM achieves the same target BER as conventional OFDM while requiring approximately 2–4 dB lower SNR, corresponding to reduced transmit power or improved reliability under identical channel conditions, 16—50% higher energy efficiency depending on modulation order, and significantly reduced out-of-band emissions due to its inherent partial activation of its subcarrier. Importantly, these gains are obtained without increasing transmit power or the occupied bandwidth and with only moderate receiver complexity. Overall, the findings establish OFDM-IM as a strong and practical candidate waveform for 6G networks, offering a balanced trade-off between performance gains and implementation complexity. Future work will extend this framework to doubly dispersive and terahertz channels, massive MIMO configurations, reconfigurable intelligent surface (RIS)-assisted systems[21], and hybrid multiple-access techniques, further strengthening the role of index modulation in next-generation wireless communication systems.

References

[1] A. Gupta and R. K. Jha, "A survey of 5G network: Architecture and emerging technologies," *IEEE Access*, vol. 3, pp. 1206–1232, 2015, doi: 10.1109/ACCESS.2015.2461602.

[2] M. Shafi *et al.*, "5G: A tutorial overview of standards, trials, challenges, deployment, and practice," *IEEE J. Sel. Areas Commun.*, vol. 35, no. 6, pp. 1201–1221, Jun. 2017, doi: 10.1109/JSAC.2017.2692307.

[3] T. S. Rappaport *et al.*, "Millimeter wave mobile communications for 5G cellular: It will work!," *IEEE Access*, vol. 1, pp. 335–349, 2013, doi: 10.1109/ACCESS.2013.2260813.

[4] K.-H. Kim, "Dither signal design for PAPR reduction in OFDM-IM over a Rayleigh fading channel," *IEICE Transactions on Communications*, vol. 107, no. 7, pp. 505–512, 2024.

[5] J. Zhu, Q. Luo, G. Chen, P. Xiao, and L. Xiao, "Design and performance analysis of index modulation empowered AFDM system," *IEEE Wireless Communications Letters*, vol. 13, no. 3, pp. 686–690, Mar. 2023.

[6] W. Jin, M. Wang, G. Yang, and Z. Chen, "Energy-efficient and fading-resistant multi-mode OFDM-IM with high dimensional mapping," *IEEE Transactions on Wireless Communications*, vol. 22, no. 8, pp. 5005–5017, Aug. 2022.

[7] D. Khosla, S. Singh, R. Singh, and S. Goyal, "OFDM modulation technique & its applications: a review," in *International Conference on Innovations in Computing (ICIC 2017)*, 2017, pp. 101–105.

[8] M. A. Abdeltwab, K. ElBarbary, and A. Elhenawy, "Performance Improvement of Coded OFDM Communication System in AWGN Channel," *International Journal of Computer Applications*, vol. 110, no. 11, pp. 17–23, 2015.

[9] X. Feng, Z. Zhao, Y. Zhao, Z. Zhao, L. Meng, and Y. L. Guan, "OFDM-Based Waveform Design for MIMO DFRC Systems With Reduced Range Sidelobes: A Majorization-Minimization Approach," *IEEE Trans. Veh. Technol.*, vol. 74, no. 3, pp. 4582–4595, Mar. 2025.

[10] Y. Lian, X. Bi, P. Zhao, and Y. Jiang, "A research on modulation and detection in OFDM-IM system," in *Proc. 3rd Asia-Pacific Conf. on Communications Technology and Computer Science (ACCTCS)*, IEEE, 2023, pp. 27–33.

[11] K. Acharjya and K. Suneetha, "Examining and comparing: Performance of OFDM utilised in 6G communication," in *Proc. 1st Int. Conf. on Advances in Computer Science, Electrical, Electronics, and Communication Technologies (CE2CT)*, IEEE, 2025, pp. 526–530.

[12] M. Awais, M. S. Sarwar, S. Y. Shin, and Y. H. Kim, "Enhanced signal detection for low-order modulated OFDM-IM via deep learning," in *Proc. 15th Int. Conf. on Information and Communication Technology Convergence (ICTC)*, IEEE, 2024, pp. 1888–1890.

[13] P. Lavanya and G. S. S. Varma, "IM-NOMA: A Hybrid OFDM-IM and OFDM Systems for Enhancing Achievable Rate and SNR with QPSK," in *2024 Third International Conference on Electrical, Electronics, Information and Communication Technologies (ICEEICT)*, IEEE, 2024, pp. 1–5.

[14] B. Zheng, M. Wen, E. Basar, and F. Chen, "Multiple-input multiple-output OFDM with index modulation: Low-complexity detector design," *IEEE Transactions on Signal Processing*, vol. 65, no. 11, pp. 2758–2772, 2017.

[15] E. Basar, M. Wen, R. Mesleh, M. Di Renzo, Y. Xiao, and H. Haas, "Index modulation techniques for next-generation wireless networks," *IEEE Access*, vol. 5, pp. 16693–16746, 2017.

[16] E. Başar, "Multiple-input multiple-output OFDM with index modulation," *IEEE Signal Processing Letters*, vol. 22, no. 12, pp. 2259–2263, 2015.

[17] T. Liu, "A review on the 5G enhanced OFDM modulation technique," in *Proc. 3rd Asia-Pac. Conf. Commun. Technol. Comput. Sci. (ACCTCS)*, Shenyang, China, 2023, pp. 677–683, doi: 10.1109/ACCTCS58815.2023.00128.

[18] R. Makkar, M. Jain, S. Soni, D. Rawal, and N. Sharma, "On performance of cooperative OFDM system with subcarrier number modulation," in *Proc. IEEE Wireless Commun. Netw. Conf. (WCNC)*, 2024, pp. 1–5.

[19] Y. Xiao and P. Cheng, "Identification of OFDM and OFDM-IM Signals Using Statistical and Machine Learning Methods," in *2025 IEEE 26th International Workshop on Signal Processing and Artificial Intelligence for Wireless Communications (SPAWC)*, IEEE, 2025, pp. 1–5.

[20] L. Zhang, A. Ijaz, P. Xiao, M. M. Molu, and R. Tafazolli, "Filtered OFDM systems, algorithms, and performance analysis for 5G and beyond," *IEEE Transactions on Communications*, vol. 66, no. 3, pp. 1205–1218, 2017.

[21] X. Ma, Y. Zhao, H. Zhang, Y. L. Guan, and C. Yuen, "Joint Precoder and Reflector Design for RIS-Assisted Multi-User OAM Communication Systems," *IEEE Trans. Wireless Commun.*, vol. 25, pp. 618–630, 2026.